Strojniški vestnik - Journal of Mechanical Engineering 55(2009)1, 5-14
UDC 621.833.38
Paper received: 15.12.2008
Paper accepted: 09.02.2009

Cylindrical Wormgearings with Progressively Curved Shape of Teeth Flanks

Gorazd Hlebanja[1,*] - Jože Hlebanja[1] - Miro Čarman[2]
[1] University of Ljubljana, Faculty of Mechanical Engineering
[2] Fotona d.d., Ljubljana

A wormgearing or a worm gear set, featuring concavely shaped worm contact flanks and convex worm gear teeth is proposed in this paper. Corresponding flank profiles are defined by a mathematical function enabling progressive curvatures of profiles. This function is used to define a basic worm profile in the axial plane, wherefrom worm flank surface and mating worm gear profile and flank surface are derived. Furthermore, cutting tools for manufacturing such wormgearing are defined. Kinematic circumstances are discussed in detail, thus disclosing the emergence of contact lines (surfaces). The essential characteristics of the proposed wormgearing are that its entire teeth flank surfaces in contact are involved in power transmission and that concave-convex contacts exist anywhere on flank surfaces. Thus, improved properties in power transmission and lubrication can be expected, consequently resulting in lower energy losses and lower wear.

Keywords: gears, worm gearings, power transmission

0 INTRODUCTION

Wormgearings are technical devices which date back to the time of Archimedes [1]. Worm drives are often employed in various applications, e.g. elevators, conveyors, presses, rolling mills, mining industry machines, rudders, and manufacturing machines [2] to [6]. The advantage of worm gearboxes is that they allow a rather high reduction of the rotational speed in the smallest possible space. Modern worm gears are increasingly used in machine-tool positioning tables, cutter drives in milling machines, robotics etc. Rotary tables can be equipped with precision duplex wormgearings with adjustable backlash. Continuous improvements in production methods implicate that worm gears can perform precision tasks and have led to greater efficiency in their performance. High-precision wormgearings are also produced for mechanical drives in automotive equipment [3] to [6]. This is one of the reasons why new worm-gear producers emerge. This is also true for continuous improvements in gear toothing and development of new gear-production and testing machines.

1. ZA-worm gear set, where the shape of worm gear (pair) teeth flanks is defined by a turning cutter profile, which is trapezoidal in the worm's axial plane.
2. ZN-worm gear set, where the shape of worm gear (pair) teeth flanks is defined by a turning cutter profile, which is trapezoidal in the worm's normal plane.
3. ZK-worm gear set, where a gearing cutting tool is shaped as a double truncated zone (milling and grinding plate), and its axis is turned against the worm axis for the angle defining a pitch of the worm helix.
4. ZI-worm gear set where a worm is essentially an involute gear with the inclination angle which is complementary to the pitch of its helix; teeth flanks in their front view are involute in this case.
5. ZH-worm gear set is characterized by a concave circular worm teeth shape and complementary convex worm gear teeth enabling concave-convex contact; these bear the Cavex trademark under the Flender company [4].
6. Holroyd worm gear set is characterized by a special shape (based on an involute tooth, British standard 7121 [3]) of the worm thread and corresponding worm gear teeth shape; this shape type enables better contact between teeth flanks and thus better lubrication.
7. ZS-worm gear set, where teeth flanks are defined by a specially (S-shaped) designed path of contact [12].

*Corr. Author's Address: University of Ljubljana, Faculty of Mechanical Engineering, Aškerčeva 6, 1000 Ljubljana, Slovenia, gorazd.hlebanja@fs.uni-lj.si

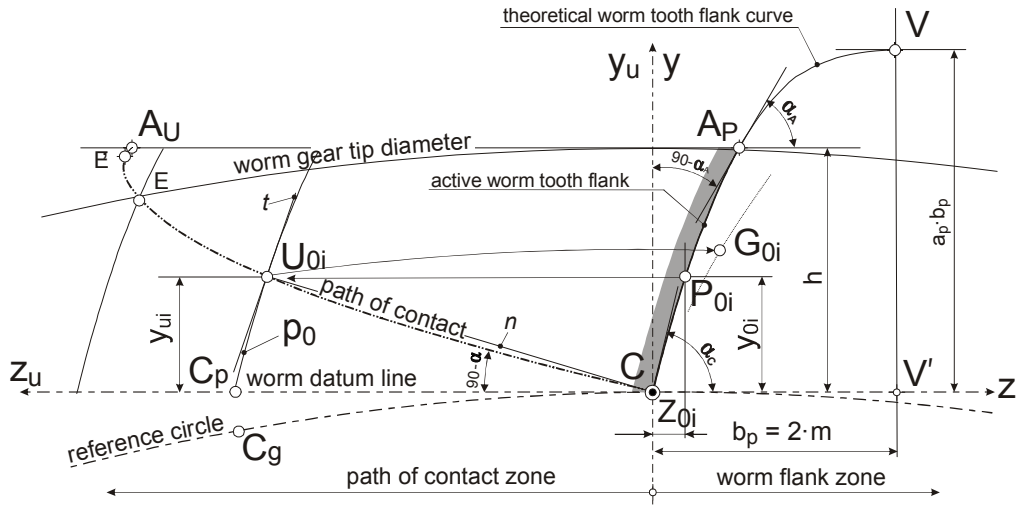

Fig. 1. *The worm tooth basic profile and the corresponding path of contact in the axial section*

This paper presents some new possibilities in this area. In this respect a wormgearing arrangement with a specially shaped toothing is proposed, featuring an improved concave–convex alignment.

1 WORM TOOTH PROFILE

The proposed wormgearing has been developed based on experience with external and internal spur gears formed with a curved path of contact [7] to [10]. A worm tooth shape is defined in the worm's axial plane by the following mathematical expression:

$$y = a_p \cdot b_p \cdot \left[1 - \left(1 - \frac{z}{b_p} \right)^n \right] \tag{1}$$

where y and z are Cartesian coordinates, a_p is the height factor, b_p is the width factor, and n stands for power exponent.

Eq. (1) represents a generalized higher order parabola. Figure 1 depicts the parabola's point of origin, which coincides with pitch point C and its top in V. The factors a_p, b_p, and n should be selected according to the required characteristics of the chosen wormgearing. The lower part of the parabola, the part CA_P, defines the flank of the worm tooth in the axial plane.

Gear size is usually defined by its modulus m, the tooth pitch p on the reference circle (i.e., the datum circle) divided by π. This is why it seems reasonable to develop the worm tooth flank shapes of uniform sizes for any standard modulus m, including for wormgearings discussed in this paper. Thus, the proportion between the tooth pitch p and its height h, as well as the space width e and the tooth thickness s should be adopted a priori. However, in order to meet the design criteria, to attain wormgearing's desired performance, parameter selection seems sensible. In this context the height factor a_p, the width factor b_p, and the power n serve to obtain an apropriate tangent inclination range of a worm tooth flank and appropriate curvature radii. The worm-tooth profile represented in Fig. 1 was designed with a tangent of inclination alteration and with a radius of curvature ρ alteration as presented in the diagrams in Fig. 2.

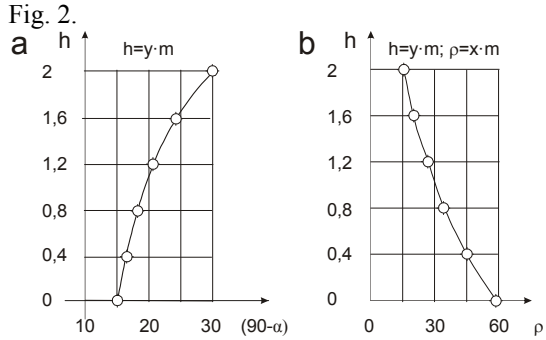

Fig. 2. *Properties of the tooth profile: a) tangent of inclination α; b) radius of curvature ρ*

Thus, the inclination of the tangent of the worm-tooth profile α is diminished gradually from the initial 75º at the tooth top in the pitch point C to approximately 60^0 at the tooth bottom in the point A_P as illustrated in Fig. 2a. Similarly, the radius

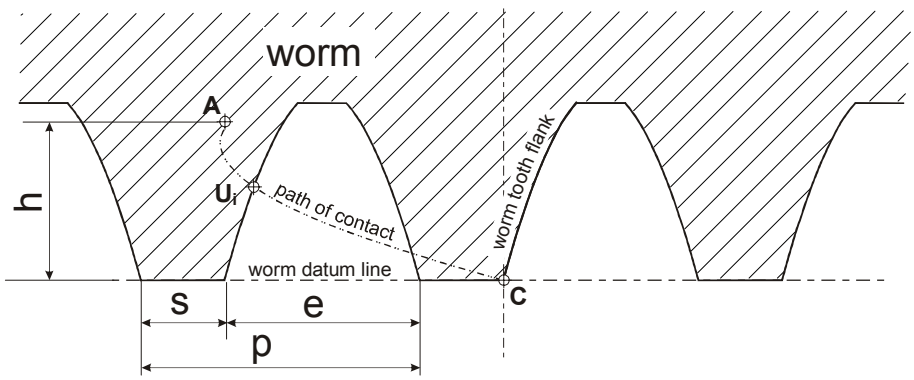

Fig. 3. *Cross-section of a worm in the axial plane*

of concave curvature ρ decreases from its maximum at the tooth top in the point C to its minimum at the tooth bottom in the point A_P as shown in Fig.2b.

The path of contact is generated by a trace of the contact point U_{0i} of the driving worm tooth flank and the driven worm gear tooth flank surfaces. The contact point U_{0i} moves from the starting point A_U to the end point, which is in the pitch point C, as illustrated in Fig. 3. For each point P_{0i}, arbitrarily selected on the worm-tooth profile, there is exactly one point U_{0i} in the path of contact, both having the same ordinate y_{0i} and abscissa z_{Ui} values, the latter defined by $z=y\cot\alpha$. If the tooth flank profile (with the point P_{0i}) is translated horizontally up to the point U_{0i}, then its normal n to the tangent (to the tooth flank) t in the point U_{0i} runs through the pitch point C. Rotation of U_{0i} around the worm gear axis provides the point G_{0i} located on the worm gear tooth flank. A worm gear flank could also be generated so that for each point P_{0i} of a basic worm tooth profile there is the point U_{0i} on the path of contact, wherefrom the point G_{0i} rotates and shapes a worm gear tooth profile. A progressively curved profile of the basic worm-tooth profile (see Fig. 3) implies progressive curvature of the path of contact.

Following the basic worm tooth profile as shown in Fig. 1, specific teeth size should be defined appropriately in the axial plane. Thus, for the tooth tip thickness $s=0.3\cdot p$ and for the tooth space width $e=0.7\cdot p$ were selected, where the tooth pitch is $p=\pi\cdot m$. Like in spur gears where a basic rack profile is defined, the worm profile (Fig. 3) could in principle be used as a basic rack profile defining the shape of the worm gears as illustrated in Fig. 4. In this arrangement the worm datum line is placed at the worm tooth tip, thus the rack profile rotation along the worm gear reference circle initiates worm gear flanks, particularly inter gear movement in the pitch point C effects by pure rolling.

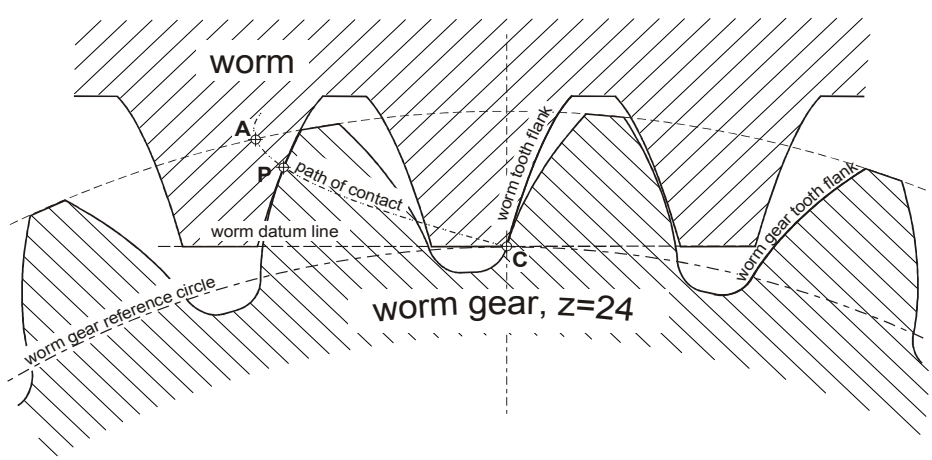

Fig. 4. *Mating worm and worm-gear in the axial plane*

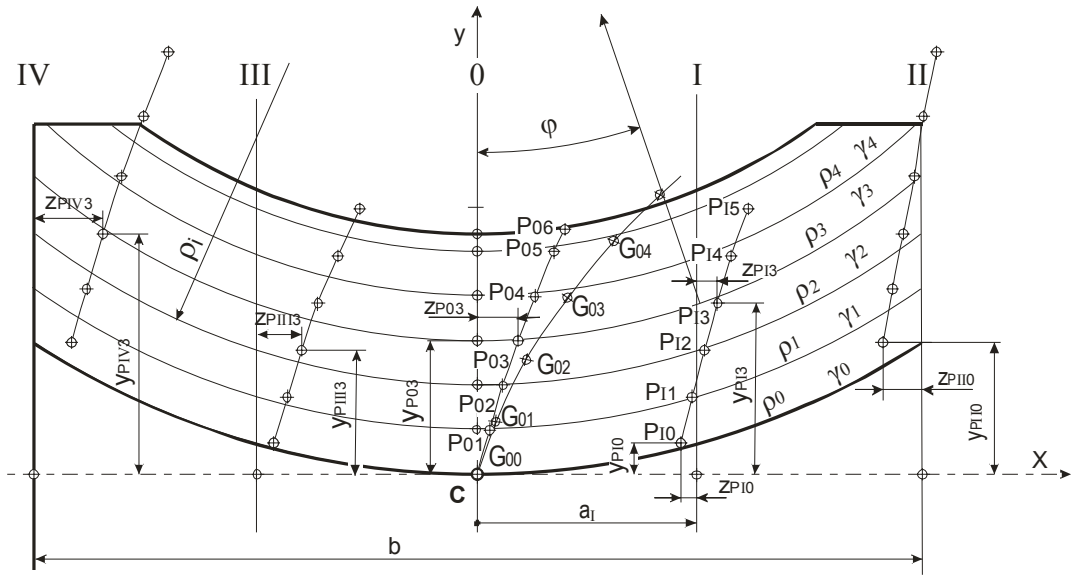

Fig. 5. *Axial view of the worm tooth flank including helix lines and worm tooth profiles in parallel planes*

2 WORM AND WORM-GEAR PROFILES

The worm and worm-tooth profiles in the worm-axis plane have been defined in the previous section with Fig. 3 illustrating the rack profile and Fig. 4 a wormgearing. The next question to be addressed is the definition of the worm and worm gear teeth profiles in planes parallel to the *y-z* plane, i.e. the worm axis plane. The starting point is the basic worm tooth profile defined by Eq. (1) and the corresponding worm gear tooth profile, both located on the worm axis plane. One can observe the points from P_{00} to P_{06} relating to the first and each point of corresponding helical lines in Fig. 5. These helical lines could be regarded as infinitesimally small helical surfaces whose projections in the axial direction are circular arcs with radii ρ_i and helical angle γ_i. The corresponding worm gear tooth profile, designated by points G_{00} to G_{04} is also illustrated in Fig. 5.

Helical lines also correspond to the cutting manufacturing process. Therefore, it could be stated that a helical line belongs to each point of the basic worm tooth profile and that there is a

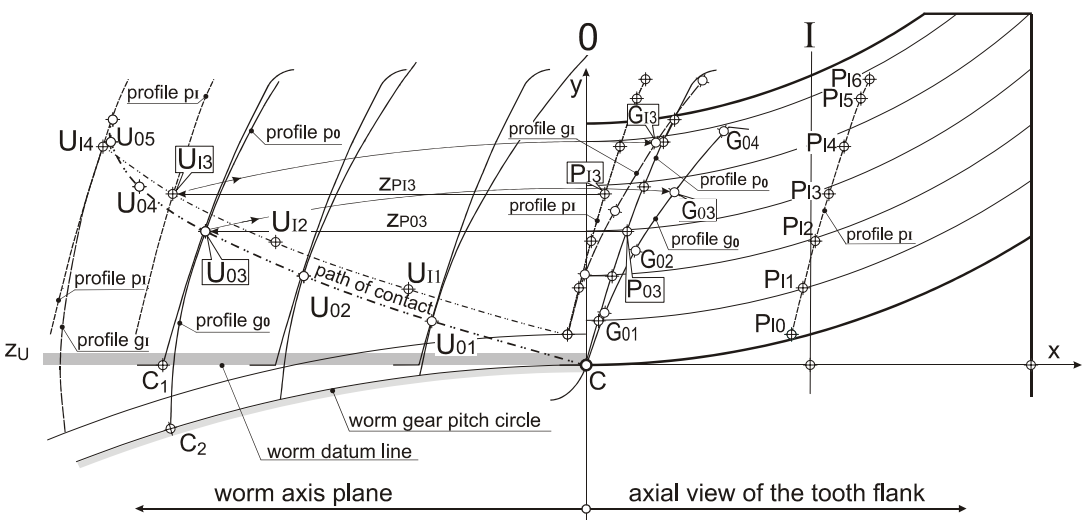

Fig. 6. *Worm gear profile generation in parallel planes*

contact point on the worm tooth profile in any parallel plane for each helical line. This way, any P_{0i} could be transformed to a corresponding point of the worm tooth profile in an arbitrary parallel plane; e.g. the helical line 3 runs through P_{03} on the basic profile and through P_{I3} on the parallel plane I and also through the corresponding points on the parallel planes II, III and IV. Thus, P_{03} coordinates in the x-y plane are x_{P03} and y_{P03}, and those of P_{I3} are x_{PI3} and y_{PI3}. A particular helical line is the basic line laid on the worm tip cylinder and running through the pitch point C. The basic helical line has the curvature radius ρ_0 in x-y plane and the lead angle γ_0. Its axial pitch is $p_0 = 2\ \pi\ \rho_0 \tan\gamma_0$. Any other helical line can be derived out of the basic helix; however, by using an appropriate radius ρ_i and a lead angle γ_i. An arbitrary point of the worm tooth could be computed in this way. Thus

$$y_{Pki} = y_{P0i} - \rho_i(1-\cos\omega_i) \text{ and}$$
$$z_{Pki} = z_{P0i} - \rho_i\ \omega_i \tan\gamma_i \qquad (2)$$

are the coordinates of an arbitrary point P_{ki}, where k is the index of a parallel plane (x direction) and i the index in y direction; also $\sin\omega_i = a_k/\rho_i$.

Meshing is possible when its counterpart worm gear tooth profile exists for a particular worm tooth. Accordingly, each worm tooth profile p_k in a parallel plane conjugates with a worm gear tooth profile g_k. Definition of such a profile g_k in the plane K is based on the prior knowledge of its counterpart p_k, which also implies identifying both basic profiles, namely p_0 and g_0, and the path of contact in the worm axis plane as observed in Fig. 6. The right side of Fig. 6 shows the axial view of the worm tooth flank profile p_0 (z-y plane 0) and the profile p_I (parallel z-y plane I), both in the revolved section. The left side, on the other hand, portrays the front view – the worm axis plane, where worm gear tooth profile generation is illustrated.

As illustrated in Fig. 1, there is a point on the path of contact for every point of the basic worm tooth profile, the meshing point U_{0i} of the worm tooth profile p_0 and the worm gear tooth profile g_0. Therefore, U_{0i} is the contact point where P_{0i} on p_0 and G_{0i} on g_0 coincide. Since the point U_{0i} is translated in the z-axis direction against the coordinate system origin C, this also implies that the worm profile point P_{0i} is also shifted for z_{P0i} to U_{0i}. Moreover, pure rotation in the opposite direction (without sliding between the worm datum line and the worm gear pitch circle) around the worm gear axis from the point U_{0i} for an arc length corresponding to the translation distance defines the point G_{0i} on the basic worm gear profile; e.g. the point P_{03} on the worm basic tooth profile p_0 is moved for z_{P03} to U_{03} and rotation from there for the arc length $\widehat{CC}_1 (= \widehat{CC}_2)$ yields the point G_{03}. Any worm tooth profile p_k in any parallel plane belongs to the same worm helical surface; therefore, any geometrical or kinematic relation of such a profile to other gear elements can be calculated either analytically or graphically.

The estimation of profiles in any parallel plane k is similar to the estimation procedure for the path of contact and the teeth profiles in the worm axial plane. Thus, the point P_{ki} is transformed in the axial direction for the distance z_{Pki}, which is modified due to the changed radius of

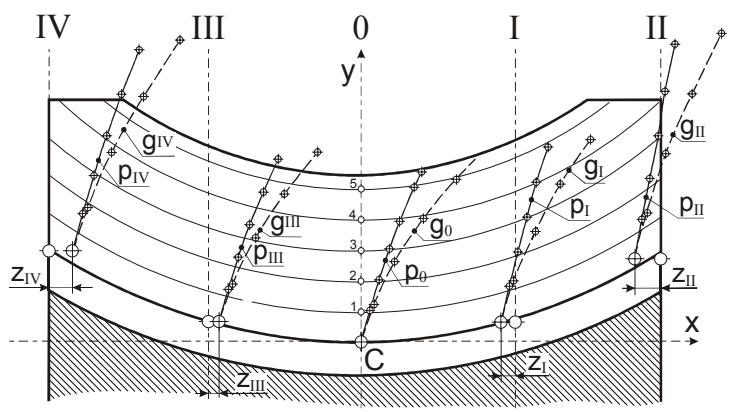

g_k - worm gear tooth profile
p_k - worm tooth profile

Fig. 7. *Worm and worm gear profiles in parallel planes*

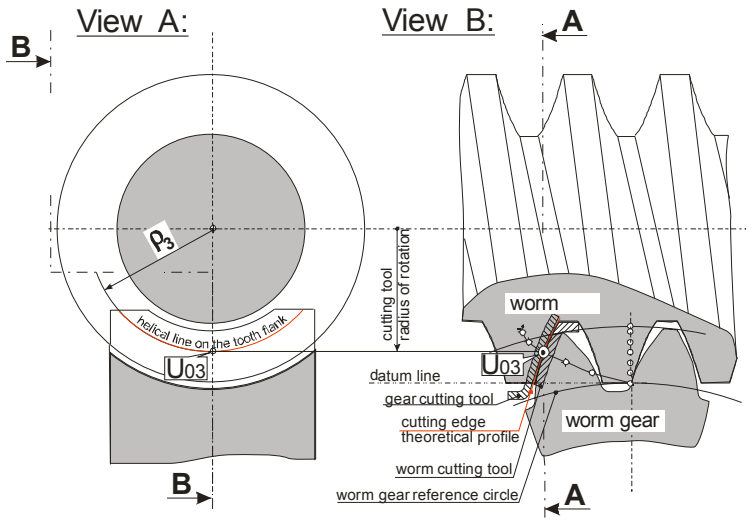

Fig. 8. *Contact between the worm tooth and worm-gear teeth flanks under manufacturing conditions*

rotation, to the point U_{ki}, and rotated from there around the worm gear axis O_2 to the point G_{ki} on the profile g_k. As illustrated in Fig. 6, the point P_{I3} is shifted to U_{I3} for z_{PI3} and rotated to G_{I3} located on the tooth profile of the worm gear in the parallel section - the plane I. Fig. 7 shows profiles of both, the worm and the worm gear in the axial plane and parallel planes I, II, III and IV.

3 MANUFACTURING PROCESS OF CONVEX-CONCAVELY SHAPED WORM GEARS

The manufacturing process of worm gear tooth profiles is based on the fact that a gear cutting edge point can be defined for each point of the path of contact. The cutting edge point forms a helical line on a worm tooth. Consequently, it forms a worm tooth surface when moved in the axial direction, while at the same time a worm rotates in a synchronized manner.

As illustrated in Fig. 8, the point U_{03} matches the coinciding helical line of the worm and the helical line of the worm gear. The point U_{03} itself is on the path of contact. The corresponding helical lines on both teeth represent the trails of points on cutting tools edges. Although the helical lines overlap, relative motions of corresponding cutting edges against the corresponding teeth flank surfaces differ. The worm tooth flank acquires its shape when a cutting tool proceeds over the worm's helical line, whereas the worm gear tooth shape emerges by newly generated contact lines due to the relative motion between the work-piece and the tool, which is illustrated in Fig. 10. The cutting edge indicated as G in Fig. 10 moves, e.g. along the helical line no. 3 from the right to the left for a left winded worm, and shapes a contact line on the worm gear tooth flank.

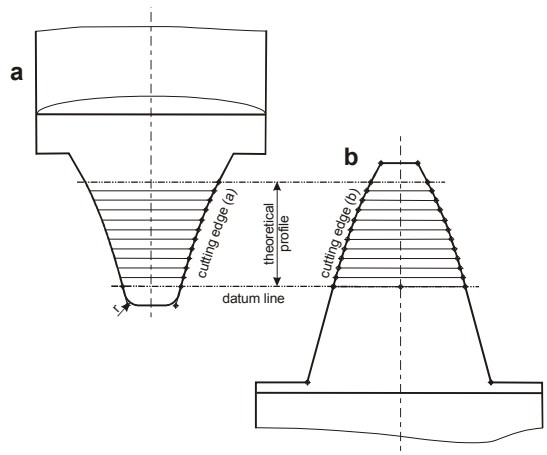

Fig. 9. *Cutting tool profiles in the normal section: a) gear cutting tool profile, b) wormcutting tool profile*

Various types of machines and processes can be employed in worm and worm gear manufacturing; however, always by using tools with appropriate cutting edge profiles. The cutting tool profiles for the proposed wormgearings are illustrated in Fig. 9. They are characterized by the identical cutting edges (Fig. 8 – view B); however, one is concave and the other convex, the former for a worm gear (Fig. 9a) and the latter

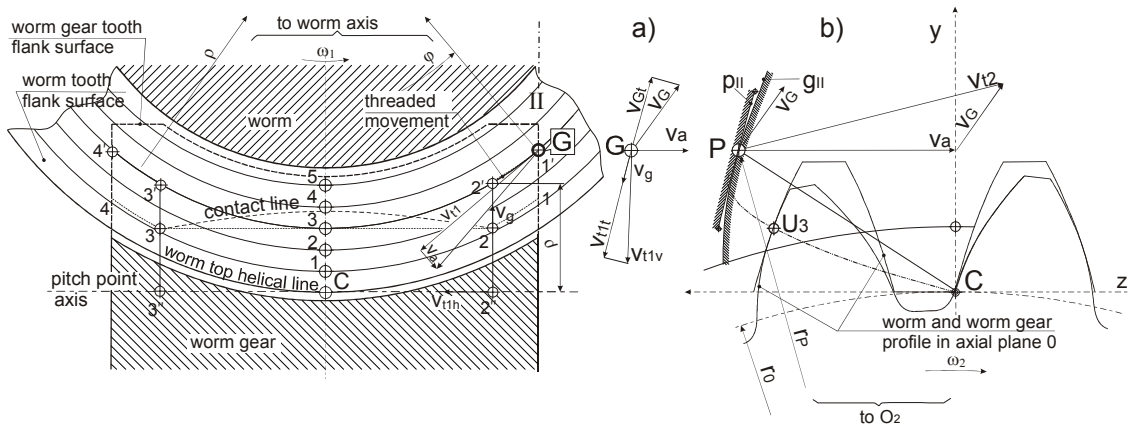

Fig. 10. *Formation of contact lines*

(Fig. 9b) for a worm. The profiles of the cutting edges are positioned in y-direction in accordance with the worm datum line and oriented as the profiles of the worm tooth and the worm-gear teeth are oriented in the working position.

Fig.10 reveals velocity circumstances of an arbitrary cutting edge designated by G, which is, for the purpose of illustration, positioned at the worm's outer limit (coincident with the parallel plane II) and on the helical line no. 3. Fig 10a points out the velocity circumstances of the cutting edge G, whereas Fig 10b indicates velocities of the worm gear flank in the axial parallel plane II. It should be noted that the worm tooth flank is exposed in the axial view and covers the worm gear tooth flank. However, visible helical lines overlap for both meshing flanks. The cutting edge G rotates around the worm axis with a tangential velocity

$$v_{t1} = \varpi_1 3\rho_3, \tag{3}$$

where its axial component (in z direction) is

$$v_a = v_{t1}.\tan\gamma_3. \tag{4}$$

The latter i.e. the system speed of the worm gear, is constant over the entire contact area, while a magnitude of the tangential velocity is constant for any particular helical line.

Fig.10a also demonstrates a vertical component of the tangential velocity v_{t1} (y direction)

$$v_{t1v} = v_{t1}.\sin\,\omega \tag{5}$$

and its horizontal component

$$v_{t1h} = v_{t1}.\cos\,\omega. \tag{6}$$

Therefore, the relative velocity v_G signifying rotational speed of the cutting edge G around the pitch point C in parallel plane II is

$$v_G = \omega_2 \times \overline{CP}. \tag{7}$$

The relation ϖ_1/ϖ_2 stands for the transmission ratio of a wormgearing. The cutting edge G contacts the worm gear tooth flank at point P, located on the tooth flank profile p_{II} (see Fig. 7). This is the point where sliding between the worm gear tooth flank and its counterpart worm flank originates in a common tangential direction. The velocity components v_{t1t} and v_{Gt}, are in P oriented in opposite directions. Their difference is v_g denoting the cutting edge velocity against the worm gear tooth flank velocity, or the sliding velocity of teeth flanks relatively to each other.

Relative velocity is in this case the velocity of the worm tooth flank (regarded as the cutting tool edge) opposite to the worm gear tooth flank. The components of v_g are v_{t1h} and v_a, also the system velocity. Due to the rotation of the cutting tool edge, the tangential velocity v_{t1} direction varies, its horizontal v_{t1h} and vertical component v_{t1v} are modified as well with the former having its maximum value in the axial plane and the latter at the contact starting point.

Velocity circumstances in the axial cross-section are revealed in Fig. 10b. The discussed wormgearing is presented in the worm axial plane 0, where the point U_{03} on the path of contact is located, and in the parallel plane II, where the point P and cutting tool edge G coincide. The point P on the worm gear tooth flank rotates around the gear axis O_2 with the tangential velocity $v_{t2} = \varpi_2 3r_P$, and translates in the axial direction with the velocity v_a. These two cases are significant in this context:

– if v_{t1t} is greater than v_{Gt} in magnitude, $|v_{tvt}| > |v_{Gt}|$, than power transmission between the worm and the worm gear acts like a screw

and a nut – thread like or threaded movement.
- When the condition $v_{tvt} = v_{Gt}$ is met, then threaded movement reverts to sliding and
- sliding movement if $|v_{tvt}| < |v_{Gt}|$; in this period the cutting tool edge moves perpendicular to the pitch point axis with the velocity $v_g = |v_{tvt}| - |v_{Gt}|$.

Based on the above considerations the contact between the worm helical line and the worm gear tooth flank can be reconstructed. Such a worm gear contact line is represented in Fig. 10, in the worm axial view, for the worm helical line no. 3. In this case the contact starts at the point labelled as "1" and moves to "2" in a thread-like manner. From there the sliding movement continues to "3" and finally, a threaded movement prolongs to the point "4". It can be observed that by approaching the helical lines to the pitch point C, threaded zones are increasing from both sides and sliding zones are vanishing. The top worm helical line contact enables pure threaded movement, provided that it runs through C.

4 MANUFACTURED WORMGEARING

The manufacturing method described above has been used to implement an experimental worm gearing, to assemble it in an apropriate housing and to verify such an arrangement in proper working conditions. Thus, such a worm gearing, Fig. 11, with module m=3 mm and axial distance a=50 mm consisting of a single threaded worm and a worm gear with $z_2 = 21$ was produced and assembled in a standard housing of a Hydro-Mec s.p.a. The gear set was successfully tested under load and the teeth flanks did not suffer any considerable damage.

A 3D ACIS Modeller was employed to define contact lines of a worm gearing and ProEngineer Wildfire was used to visualize contact surfaces as illustrated in Fig. 12. One can observe evident separated sliding and treaded movement zones, which confirms theoretical considerations. The lines (surfaces) near the top worm gear circle are separated. Also, the contact lines (surfaces) are space curves (surfaces) and the crossing between zones is continuous. Load distribution through the entire worm teeth flanks area can be expected assuming manufacturing process of a sufficient accuracy and appropriate stiffness.

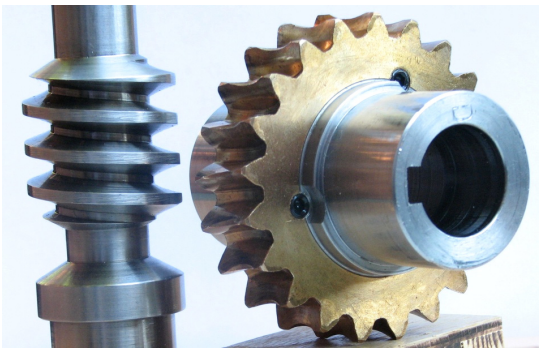

Fig. 11. *Wormgearing with m= 3 mm, z2 = 21, a = 50 mm*

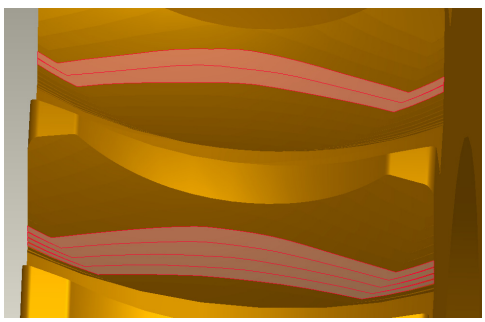

Fig. 12. *Computer modelled contact surfaces of a worm gear*

5 EHD LUBRICATION PROPERTIES

Worm gears are prevailingly used for power transmission from a fast rotating electromotor to a slow speed working machine. For this, two possible lubrication systems exist; either a worm or worm gear should be sunk in the oil contained in a gear box.

In both cases, the lubricating fluid soaks the teeth flanks and transmits oil to the entry opening preceding a contact line as illustrated in Fig. 13. The oil is transported to the contact surfaces by the half sliding velocity v_g and the condition for EHD lubrication is fulfilled. As Fig. 12 shows, individual contact lines are extended over the entire gear width. Therefore, it could be anticipated that the oil gap preceding the entry opening exists over the entire gear width, as illustrated in Fig. 14.

Power transmission from a worm flank to a worm gear flank is transmitted continuously from one contact line to the other and from the path of the contact start to its end in the pitch point C. The important conditions for EHD lubrication are sliding velocity v_g and wedge shaped inlet space between lubricated surfaces. In this

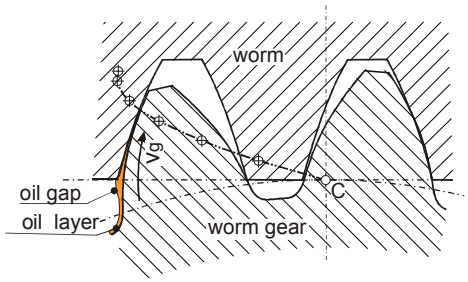

Fig. 13. *Forming of oil lubrication film between teeth flanks*

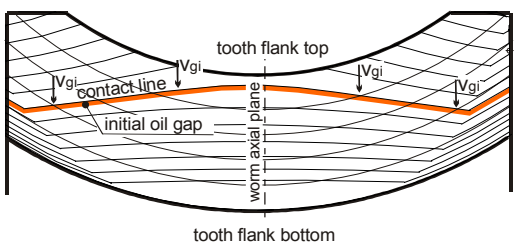

Fig. 14. *Lubrication conditions*

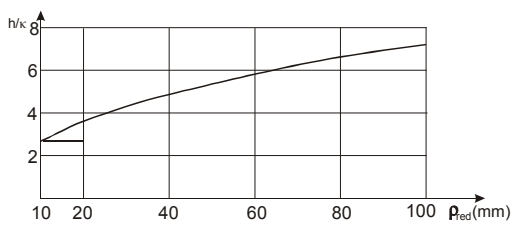

Fig. 15. *Functional dependence of oil film thickness on* ρ_{red}

case, such conditions exist only over the sliding zone. However, the sliding direction of both contacting surfaces are parallel in treaded movement zone, thus the conditions for EHD are not fulfilled. Nevertheless, surfaces are lubricated similarly to conditions in spindle and nut contact.

6 CHARACTERISTIC ELEMENTS FOR EVALUATION

Knowing the benefits of the concave–convex shaped gear teeth contact with regard to EHD lubrication, it seems reasonable to estimate the weight of the main influencing factors in oil film formation between teeth surfaces. These factors are defined by the widely used Dowson Higginson's experimental relation [11] for the oil film thickness *h:*

$$h = 1.6\alpha^{0.6}\left(\eta_0 \cdot u\right)^{0.7}\left(E'\right)^{0.03} w^{-0.13}\rho_{red}^{\ 0.43}. \quad (8)$$

Thus, oil viscosity η_0 and average velocity u of surfaces in contact have the highest impact, followed by contact geometry defined by a reduced radius of curvature ρ_{red} in each contact point, whereas specific contact load (per length unit) w and material (E') have only modest or low influence on the oil film thickness.

Specific contact load w depends on the load and contact line length over the entire worm gear width. This includes both, the sliding and the threaded movement zones. Power transmission acts in both zones, whereas EHD lubrication is active only in the former. The specific contact load should be calculated considering the entire contact width. The benefit of the proposed wormgearing is thus lower load pressure, which implies thicker oil film thickness in the sliding zone.

The wormgearing geometry, namely the reduced radius of curvature ρ_{red} influence on the oil-film thickness is of considerable importance due to its high impact. It can be expressed by the following equation:

$$h = \kappa.\rho_{red}^{0.43} \quad (9)$$

where κ stands for

$$\kappa = 1.6\alpha^{0.6}\left(\eta_0 \cdot u\right)^{0.7}\left(E'\right)^{0.03} w^{-0.13}. \quad (10)$$

The expression κ for known parameters can be used as a normalization factor when representing functional dependence of oil film thickness on ρ_{red}, as obtained from Fig. 15.

Fig. 16 illustrates the reduced curvature radii plotted along the path of contact. Thus, the equation for ρ_{red}

$$\rho_{red} = \rho_p.\rho_g /(\rho_p-\rho_g) \quad (11)$$

contains radii of curvature in the contact ratio for a worm tooth profile – ρ_p and that of a worm gear tooth profile ρ_g.

According to the contact starting point A in Fig. 16, which reveals a high ρ_{red} in A, and considering the initial lubrication conditions one can assume the quality of lubrication conditions in A. Afterwards, the oil film thickness decreases up to the pitch point C although the contact quotient h/κ exceeds value 2 at all times. The lubrication evaluation for any parallel plane similar to that in the axial plane would reveal similar quality conditions, which indicates its quality over the entire contact area in the discussed wormgearings.

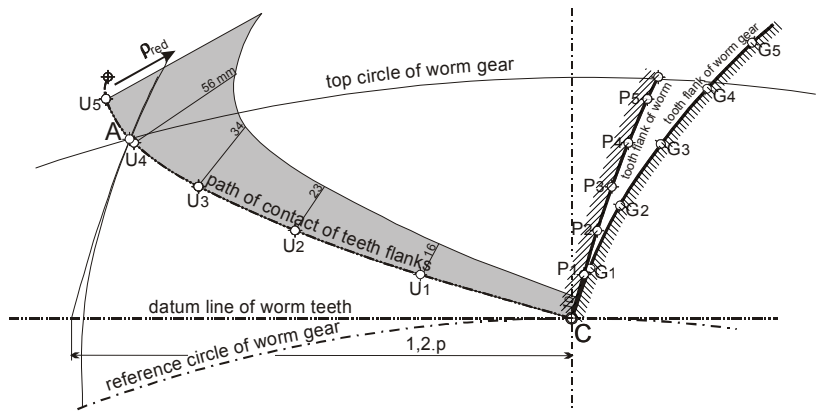

Fig. 16. *Reduced radii of curvature plotted along the path of contact*

7 CONCLUSION

The proposed approach in cylindrical worm gearings design is based on the mathematically defined worm tooth profile in the worm axial plane, wherefrom the worm gear tooth profile derives and profiles in any parallel plane can be calculated. In this way teeth flanks are defined.

Kinematic circumstances are described in detail. The cutting tools and underlying manufacturing procedure assuring proper teething are discussed as well. Therefore, the contact lines (surfaces) between worm and worm gear teeth are formed as helical lines in any contact position. The profile geometry and the latter consideration lead to a conclusion that the contact area expands over the entire contact area of both teeth flanks, which consequently implies better conditions for power transmission.

The primary feature of the proposed teeth flanks is their progressive curvature and continual concave-convex contact. Worm and worm gear meshing in such an arrangement generates a better lubricating oil film, resulting in better EHD lubrication conditions; therefore, reduced energy losses and lower wear damages are anticipated. An experimental wormgearing loaded under working conditions verified theoretical considerations. Computer simulation also confirmed the contact theory of the proposed gearing.

8 REFERENCES

[1] Seherr-Thoss, H.Chr. Graf v. (1965) *The Development of the Gearing Technology* (in German). Springer Verlag, Berlin, Heidelberg, New York, p. 48.

[2] Niemann., G., Winter, H. (1983) *Maschine Elements, Volume III* (in German). Springer Verlag, Berlin, Heidelberg, New York, Tokyo.

[3] Jüngel, H. (1992) Holroyd Tooth Profile for Wormgearings (in German). *Antriebstechnik (Mainz, 1982)*, vol. 31, no.8, p. 58-60.

[4] Flender Worm Gear Units. A.Friedr. Flender AG, http://www.flender.com/.

[5] Renold Worm Gears. Renold plc, http://www.renold.com/.

[6] Predki, W. (1995) Status of worm gear drive development, *Gear Transmissions'95,* Sofia, Bulgaria.

[7] Hlebanja, G., Hlebanja, J., Okorn, I. (2000) Research of Gears with Progressive Path of Contact. *Proceedings of DETC'00,* Baltimore, Maryland.

[8] Hlebanja, J., Hlebanja, G. (2002) Lubrication Efficiency of S-Gears. Int. Conf. on Gears, München, *VDI Berichte 1665*.

[9] Hlebanja, J., Hlebanja, G. (2005) Applicability of S-gears for Gear Trains – Advances in Non-involute Gears Development. *Antriebstechnik (Mainz, 1982)*, vol. 44, no. 2, p. 34-38.

[10] Hlebanja, G., Hlebanja, J. (2005) Tooth Flank Durability of Internal S-Gears. Int. Conf. on Gears, München, *VDI Berichte 1904*.

[11] Dowson, D., Higginson, G.R. (1977) *Elasto-Hydrodynamic Lubrication*. SI Edition. Pergamon Press, Oxford, New York, Toronto, Sydney, Paris, Frankfurt.

[12] Belšak, A., Flašker, J., Vibration Analysis to determine the Condition of Gear Units, Journal of Mechanical Engineering (2008) vol. 54, no.1, p. 11-24.